NeuroImage: Clinical 21 (2019) 101669

Contents lists available at ScienceDirect

NeuroImage: Clinical

journal homepage: www.elsevier.com/locate/ynicl

# Dynamic changes in hippocampal diffusion and kurtosis metrics following experimental mTBI correlate with glial reactivity

Kim Braeckman[a,*,1], Benedicte Descamps[a,1], Leen Pieters[b,2], Anne Vral[b,2], Karen Caeyenberghs[c,3,4], Christian Vanhove[a,1,4]

[a] Infinity Lab, Medical Imaging and Signal Processing Group, UGent, Ghent, Belgium
[b] Department of Human Structure and Repair, UGent, Ghent, Belgium
[c] Mary MacKillop Institute for Health Research, Australian Catholic University, Melbourne, VIC, Australia

ARTICLE INFO

*Keywords:*
Mild traumatic brain injury
Diffusion magnetic resonance imaging
DTI
DKI
White matter model

ABSTRACT

Diffusion magnetic resonance imaging biomarkers can provide quantifiable information of the brain tissue after a mild traumatic brain injury (mTBI). However, the commonly applied diffusion tensor imaging (DTI) model is not very specific to changes in the underlying cellular structures. To overcome these limitations, other diffusion models have recently emerged to provide a more complete view on the damage profile following TBI. In this study, we investigated longitudinal changes in advanced diffusion metrics following experimental mTBI, utilising three different diffusion models in a rat model of mTBI, including DTI, diffusion kurtosis imaging and a white matter model. Moreover, we investigated the association between the diffusion metrics with histological markers, including glial fibrillary acidic protein (GFAP), neurofilaments and synaptophysin in order to investigate specificity. Our results revealed significant decreases in mean diffusivity in the hippocampus and radial diffusivity and radial extra axonal diffusivity (RadEAD) in the cingulum one week post injury. Furthermore, correlation analysis showed that increased values of fractional anisotropy one day post injury in the hippocampus was highly correlated with GFAP reactivity three months post injury. Additionally, we observed a positive correlation between GFAP on one hand and the kurtosis parameters in the hippocampus on the other hand three months post injury. This result indicated that prolonged glial activation three months post injury is related to higher kurtosis values at later time points. In conclusion, our findings point out to the possible role of kurtosis metrics as well as metrics from the white matter model as prognostic biomarker to monitor prolonged glial reactivity and inflammatory responses after a mTBI not only at early timepoints but also several months after injury.

## 1. Introduction

Traumatic brain injury (TBI) affects yearly > 10 million people worldwide and is the leading cause of acquired disability in young adults, often caused by traffic accidents or sport injuries (Dewan et al., 2016; Thurman, 2016). Mild TBI (mTBI) is the most prevalent type of severity of TBI (about 80% of all TBI cases) and is often termed 'silent epidemic' since many patients suffer from symptoms that are not overtly visible (Bruns and Hauser, 2003). In mTBI, the brain is subjected to shear-strain forces leading to diffuse axonal injuries with most lesions emerging at the interface between brain regions with different tissue densities, such as the grey-white matter junctions (Li and Feng, 2009). Furthermore, conventional scans, such as computed tomography (CT) scans or anatomical magnetic resonance imaging (MRI) scans, often show no evidence of injury due to the diffuse and subtle nature of mTBI. Despite the lack of radiological evidence, mTBI patients suffer from cognitive deficits, such as memory problems and executive control deficits, even years after their injury (Arciniegas

* Corresponding author.
*E-mail addresses:* kim.braeckman@ugent.be (K. Braeckman), benedicte.descamps@ugent.be (B. Descamps), leen.pieters@ugent.be (L. Pieters), anne.vral@ugent.be (A. Vral), karen.caeyenberghs@acu.edu.au (K. Caeyenberghs), christian.vanhove@ugent.be (C. Vanhove).
[1] Present address: Infinity Lab, MEDISIP-IBiTech, Blok B-5 (Ingang 36), Campus UZ Gent, Corneel Heymanslaan 10, 9000 Gent, Belgium.
[2] Present address: Radiobiology Research Unit, Department of Human Structure and Repair, 6B3, Ingang 46, Campus UZ Gent, Corneel Heymanslaan 10, 9000 Gent, Belgium.
[3] Present address: Mary MacKillop Insitute for Health Research, Building 470 - Level 5 - Room 470.5.02, 215 Spring Street, Melbourne, VIC 3000, Australia.
[4] K.C. and C.V. are co-senior authors.

https://doi.org/10.1016/j.nicl.2019.101669
Received 13 August 2018; Received in revised form 4 January 2019; Accepted 5 January 2019
Available online 09 January 2019

et al., 2002). This lack of radiological evidence of brain injury has led to the application of more advanced MR imaging methods such as diffusion MRI (dMRI), that is more sensitive to assess microstructural changes following mTBI.

Diffusion MRI is an MRI technique which is being used more often the past decades due to its greater sensitivity to detect white matter changes following TBI (Basser et al., 1994; Pierpaoli and Basser, 1996). Fractional anisotropy (FA) and mean diffusivity (MD) are measures most commonly used to follow up changes in diffusion properties related to TBI (Hulkower et al., 2013). Recent dMRI reviews in mTBI described predominantly increased FA and reduced MD at acute time points (up to two weeks post injury) (Asken et al., 2018; Hulkower et al., 2013; Wallace et al., 2018). These changes in diffusion metrics have been interpreted as axonal swelling (Bazarian et al., 2012; Mayer et al., 2010). Contrary, reduced FA and increased MD values could be observed in the chronic phase of mTBI (several months after injury), possibly due to a disruption in parenchymal structure following oedema formation, axonal degeneration or fiber misalignment/disruption (Niogi et al., 2008; Rutgers et al., 2008). However, the exact time-course and cellular processes underlying alterations in diffusion metrics after sustaining brain injury are not entirely clear in human TBI and pre-injury levels are often not available.

Recently, animal TBI models have been developed to overcome these issues and enable to obtain baseline scans pre-injury. To date, there have been only a few longitudinal animal studies using a closed head impact model of mTBI, investigating brain structure alterations over time with diffusion tensor imaging (DTI) (Li et al., 2013; Singh et al., 2016; Zhuo et al., 2012). These studies provided evidence of alterations in FA and MD already detectable within a week after mTBI, however, the cellular basis of these alterations in diffusion metrics was not entirely clear.

More recently, animal studies tried to pinpoint the underlying cellular mechanisms by correlating diffusion metrics with histological markers. Several diffusion parameters could be correlated to glial fibrillary acidic protein (GFAP) (Tu et al., 2016; Zhuo et al., 2012), however it has been stated that these parameters lack specificity for histological features, despite being sensitive in detecting subtle tissue changes following brain trauma (Jones et al., 2013).

Diffusion kurtosis imaging (DKI) is an expansion of the tensor model and measures the degree of non-Gaussian diffusion which could provide additional information about tissue heterogeneity or complexity (Jensen and Helpern, 2010). Using DKI, (Grossman et al., 2013, 2012) and (Zhang et al., 2018) found reductions in MK in mTBI patients that were associated with cognitive impairments. However, DTI and DKI are only representations of the diffusion signal and aim to characterise the probabilistic water displacement profile without microstructural specificity. Microstructural mapping techniques based on biophysical models could overcome this non-specificity issue and may offer new information for describing abnormalities after mTBI (Hutchinson et al., 2018; Novikov et al., 2018). These models incorporate a-priori biological information (assumptions) into the model, to assess tissue compartments and its biological attributes more directly. For example, (Fieremans et al., 2011) recently introduced a novel white matter model (White Matter Tract Integrity model (WMTI)), which provides specific information of the intra- and extra-axonal compartments in highly aligned fiber bundles. Exchange of water molecules between these two compartments is neglected and the intra-axonal diffusivity is assumed to be lower than the extra-axonal diffusivity. It should also be noted that water trapped between the myelin sheets is not detectable with typical diffusion scanning parameters and therefore the compartment fractions correspond to measurable water fractions. The WMTI model thus estimates the axonal water fraction (AWF), axonal diffusivity ($D_a$) and the axial and radial extra-axonal diffusivity ($D_{e,||}$ and $D_{e,\perp}$). This model has already been applied on human data in many pathologies, including TBI (Chung et al., 2018; Grossman et al., 2015), multiple sclerosis (de Kouchkovsky et al., 2016), autism (Lazar et al., 2014) and Alzheimer's disease (Fieremans et al., 2013). In mTBI patients, a reduction in intra-axonal diffusivity in the splenium of the corpus callosum in mTBI patients compared to controls and was interpreted as axonal stretch injury (Chung et al., 2018). Only a few studies have applied the WMTI model in animal models. In hypomyelinated (Kelm et al., 2016) and demyelinated mouse models (Guglielmetti et al., 2016; Jelescu et al., 2016) was found that the AWF and intra-axonal diffusivity could be informative about acute inflammatory demyelination and later spontaneous re-myelinisation.

To the best of our knowledge this is the first study that applies the WMTI model in a rat model of mTBI. Also, by making use of the Marmarou weight drop model (Marmarou et al., 1994) producing a *diffuse* trauma, we believe we model the patients with no clearly visible symptoms after a mTBI much better in comparison to TBI models that produce a more focal injury (for example the controlled cortical impact model) and thus induce more moderate to severe TBI. Furthermore, the changes in diffusion metrics were obtained across time from pre-injury into the acute (one day and one week post injury) and chronic stage (three months post injury) of mTBI. In addition, we performed correlations with histology, using anti-neurofilament, anti-synaptophysin and anti-GFAP staining. This way we want to visualise whether or not the signalling of the neurons is affected (through staining of the synaptic vesicles) and complimentary the structure of the neurons (through staining of the neurofilaments). Also, the glial response, which is related to neuroinflammation, is of interest.

## 2. Materials and methods

### 2.1. Animal studies

The study was approved by the Animal Ethics Committee at the University of Ghent (ECD 15/44Aanv) and all experiments were conducted in accordance with the guidelines of the European Commission (Directive 2010/63/EU). The animals were group housed and kept under controlled laboratory conditions (12 h light/dark cycle, 20–23 °C and 40–60% humidity).

### 2.2. Induction of mild traumatic brain injury

Adult female Wistar rats ($n$ = 20, 262 ± 14 g) purchased from Janvier Labs (Le Genest-Saint-Isle, France) were divided in two groups: 10 rats that received a mild traumatic brain injury and 10 rats that did

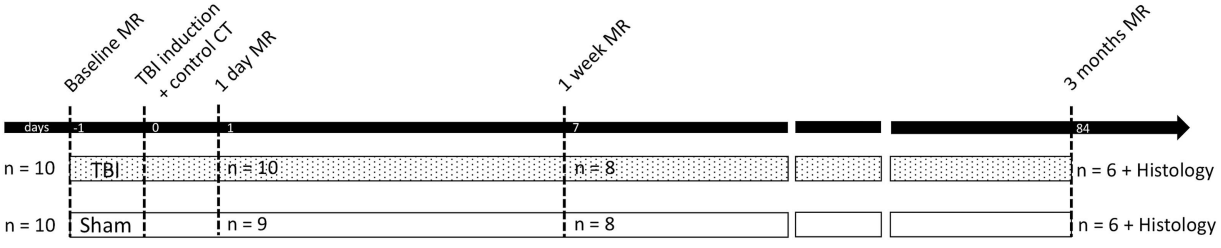


**Fig. 1.** Outline of the longitudinal scanning design.

not receive the impact (sham injury) (Fig. 1). Female rats were chosen for this longitudinal study as they are more gentile towards cage companions than males when group housed, and are expected to grow less over the time period of three months.

Mild traumatic brain injury was induced using the Marmarou weight drop model (Marmarou et al., 1994), using a multistep procedure. First, rats were anaesthetised with a mixture of isoflurane and $O_2$ (5% induction, 2% maintenance) and injected with 0.05 mg/kg buprenorphine (Temgesic, Indivior) subcutaneously. After 30 min, the rats head was shaved, 100 µl of 2% lidocaine (Xylocaine, AstraZeneca) was locally injected in the scalp and an incision was made along the centre line to expose the skull. Body temperature was maintained during surgery with a heating pad. A metallic disc with a diameter of 10 mm and 3 mm thickness, which acted as a helmet, was glued onto the skull 1/3 before and 2/3 behind bregma. Next, the rat was placed on the custom-made foam bed with a matrass of certain spring constant (Type E, Foam to Size, Ashland, Virginia, USA) and positioned directly under a Plexiglas tube with a 450 g brass weight. The rat was briefly detached from anaesthesia and the weight was dropped from a height of 1 m. Immediately after impact, the rat with the bed was moved away from the tube to prevent a second impact and the rat was reattached to the anaesthesia. To reduce the haemodynamic shock, 1 ml of physiological solution (0.9% NaCl) was injected through a catheter that was placed in the lateral tail vein. Subsequently, the helmet was removed and the incision was stitched. Then, a CT scan (X-Cube, Molecubes, Ghent, Belgium) was administered to rule out any skull fractures since this is a criterion for euthanasia. To minimize the dose, a general purpose low dose one bed position scan was performed. One day post impact the rats received an extra dose of 0.05 mg/kg buprenorphine after the MR scan.

### 2.3. In vivo longitudinal multi-shell diffusion weighted imaging

MRI data were acquired on a 7 T MRI scanner (BioSpin PharmaScan 70/16, Bruker, Ettlingen, Germany) using a volume rat brain/mouse whole body RF coil. Rats were scanned at baseline, one day, one week and three months post impact (Fig. 1). During the scanning sessions, the animals were under 2% isoflurane anaesthesia (5% for induction), body temperature was kept constant with a circulating warm water heated blanket and bubble wrap, and respiration rate was monitored with a pressure pad.

At each time point, a whole brain anatomical T2-weighted scan was acquired first using a Rapid Acquisition with Refocused Echoes (RARE) sequence: TR = 5.5 s, TE = 37 ms, RARE factor = 8, FOV = 2.5 × 2.5 cm, in plane resolution = 109 × 109 µm, 600 µm slice thickness, 45 slices, 12 min acquisition time. Diffusion images were acquired with a spin echo, echo-planar imaging (EPI) sequence between the olfactory bulb and the cerebellum. Multi-shell diffusion weighted acquisitions were recorded using an encoding scheme of 32, 46 and 64 gradient directions with b-values of 800, 1500 and 2000 s/mm$^2$ and with 5, 5 and 7 b0 images (scanned at the beginning of each shell), respectively. Other diffusion scanning parameters were as follows: TR = 6.250 s, TE = 24 ms, number of segments = 4, number of averages = 1, FOV = 3 × 3 cm, in plane resolution = 333 × 333 µm, 600 µm slice thickness, 600 µm interslice distance, 25 slices, 65 min acquisition time.

### 2.4. MRI data analysis

Diffusion weighted images (DWIs) were first corrected for noise using the *dwidenoise* function in MRtrix3 (Veraart et al., 2016, 2016). An overview of the image processing pipeline can be found in Fig. 2. Next, the images were corrected for signal drift and Gibbs ringing artefact for each shell using the ExploreDTI toolbox version 4.8.6. (Leemans et al., 2009). After concatenation of the three shells, the images were also corrected for EPI, eddy current and motion-induced geometric distortions in ExploreDTI. From the corrected DWIs, the diffusion kurtosis tensor was estimated using the weighted linear least squares method (Veraart et al., 2013). For the diffusion tensor model we obtained axial diffusivity (AD), fractional anisotropy (FA), mean diffusivity (MD), radial diffusivity (RD). The kurtosis metrics included axial kurtosis (AK), mean kurtosis (MK) and radial kurtosis (RK) and were calculated based on the diffusion kurtosis imaging model (Veraart et al., 2011). Based on a white matter diffusion model axonal water fraction (AWF), axial extra-axonal diffusivity (AxEAD), radial extra-axonal diffusivity (RadEAD), intra-axonal diffusivity (IAD) and tortuosity (TORT) were calculated (Fieremans et al., 2011). A total of 12 parametric maps were obtained for each animal at each time point.

An FA template was made in SPM 12[5] based on the local population at one week post injury. Since it is the middle time point this will ensure a good coregistration with scans of other time points (even three months post injury) before performing the volume-of-interest (VOI) analysis. To make the template first, all subjects were realigned to the first subject, after this step coregistered to the mean image of the realignment step and subsequently normalised to the mean of the coregistration step. All previously obtained parametric maps were then coregistered in SPM12 on the FA template using the FA images and a 12 parameters affine nonlinear transformation with trilinear interpolation. Next a VOI analysis was performed for the DTI and DKI parameters in the corpus callosum, hippocampus, cingulum and cortex and using the Amide toolbox (Loening and Gambhir, 2003) since these regions are closest to the impact site. Because the corpus callosum is a heterogeneous structure, this region is also subdivided in genu, body and splenium. Metrics of the white matter model were only calculated in the white matter tracts of the corpus callosum and cingulum.

### 2.5. Histological analysis

At each time point after induction of mTBI, animals were sacrificed for histological analysis (see Fig. 1 for an overview of the timeline). Specifically, 2 rats in each group were sacrificed one day and one week PI, and the remaining 12 rats were sacrificed at three months post injury. However, data collected from the rats sacrificed at the one day and one week time point are not used in this article and only results obtained from the rats euthanized three months post injury are presented here. In brief, rats were anaesthetised with 5% isoflurane in $O_2$ and received an overdose of pentobarbital intraperitoneally (> 100 mg/kg). After the breathing stopped, the animals were transcardially perfused with 4% formaldehyde following an initial flush of phosphate buffered saline (PBS). The brains were extracted from the skull and left for 2 days in the 4% formaldehyde solution. After this step, the brains were transferred to a PBS solution and embedded in paraffin.

Sections were made approximately 3.60 mm behind bregma and stained for the following cellular components: synapses (with anti-synaptophysin, SYN), glial cells (with anti-glial fibrillary acidic protein, GFAP) and neurofilaments (with anti-neurofilament, NF). Sections for SYN, GFAP or NF staining were immersed in citric acid (0.2 g/l, pH = 6), boiled in microwave for two cycles of 5 min, cooled to room temperature for 30 min and washed with PBS. Endogenous peroxidase activity was quenched with a 10 min $H_2O_2$ treatment (3%). Sections were then incubated for 30 min with normal swine serum (SYN) or normal rabbit serum (GFAP and NF), followed by incubation with the primary antibodies: rabbit monoclonal (SYN, 1/1600, 2 h, Abcam ab32127) or mouse monoclonal (GFAP, 1/400, overnight, ThermoFisher, MA5-1203; NF, 1/750, 2 h, Sigma N2912 (staining the dephosphorylated medium and heavy neurofilament chains)). Next, sections were incubated with biotinylated secondary antibodies (1/200, 30 min), streptavidin-peroxidase complex (1/200, 30 min) and 3,3′-diaminobenzidine (DAB) peroxidase solution (10 min). Finally, sections were counterstained with haematoxylin (Mayer) and coverslipped using

[5] http://www.fil.ion.ucl.ac.uk/spm/software/spm12/

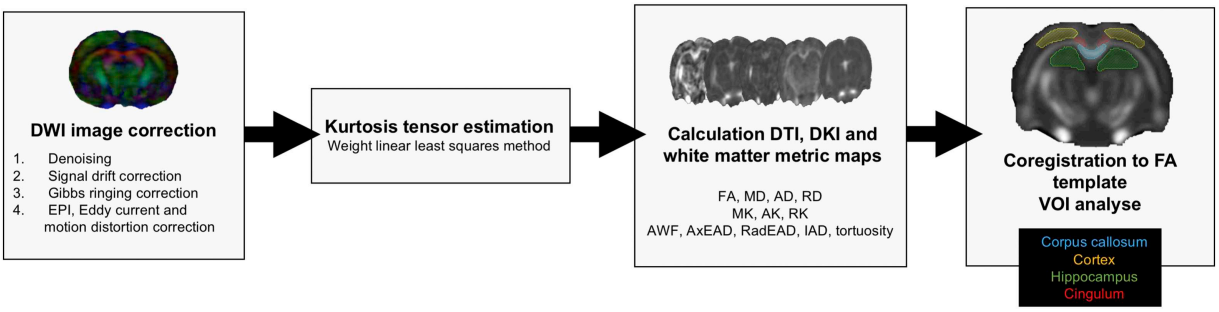


**Fig. 2.** Overview of the data processing and analysis pipeline. First, DWI images were preprocessed to correct for image artefacts. Next the kurtosis tensor was estimated and the different parametric maps calculated. Lastly, the maps were coregistered to the FA template and a VOI analysis was performed.

mounting medium (4111, Richard-Allan Scientific, Thermo Fisher Scientific) and glass coverslips (24 × 50 mm #1 (631-0146, VWR)).

All sections were digitally scanned at high resolution (40× magnification) with a virtual scanning microscope (Olympus BX51, Olympus Belgium SA/NV, Berchem, Belgium). Afterwards a different number of images was taken from sections made at the three months-time point, to cover most of the four regions of interest (corpus callosum ($n = 3$), hippocampus ($n = 8$), cingulum ($n = 2$) and cortex ($n = 4$)) at 10× magnification in OlyVIA 2.7 (Olympus Life Science) and further processed in ImageJ. For each image, first a background correction was applied with the rolling ball algorithm (radius = 50 pixels). Next, the images underwent colour deconvolution using the colour deconvolution plugin with the Haematoxyline DAB vector to obtain the image only with the DAB colour and the average pixel value was calculated. Lastly, the pixel values were calculated of a rectangular region of interest using the histogram tool. Mean and standard error values were calculated for all images and averaged within the region of interest.

### 2.6. Statistical analysis

Linear mixed model analyses were performed in SPSS Statistics 24 for each diffusion metric in each VOI (Duricki et al., 2016). We opted mixed models because these enable us to include data of subjects with missing values. The 'group' factor (TBI or sham) was included as a between-subjects variable and the factor 'time' (4 levels, baseline, one day, one week and three months post injury) as within-subject variable. Also, we used an unstructured covariance structure with no assumptions regarding the variances to allow for variable variances across time points. We corrected for multiple comparisons using Bonferroni correction, for the number of metrics within each used diffusion model. Therefore, a $p$-value $\leq .01$ was considered significant. Subsequently, post-hoc tests with Bonferroni correction were carried out to test for differences between time points or between groups.

Group comparisons of the histological markers were performed using the Mann Whitney $U$ test in SPSS Statistics 24 and a $p$-value $< .05$ was considered statistically significant. Correlation analyses were conducted between changes in diffusion MRI metrics (i.e. diffusion tensor, diffusion kurtosis and the white matter model of each time point within each VOI) and alterations in GFAP, SYN and NF reactivity of the histological sections (performed at three months post impact) using Pearson correlation coefficients. The correlations were corrected for multiple comparisons using the Benjamini-Hochberg procedure and an FDR correction of 0.10 (McDonald, 2014).

## 3. Results

### 3.1. Animals

With the exception of one animal (from the sham group), all animals survived the entire experimental period. This sole non-survivor did not wake up from anaesthesia after the baseline MRI scan. Therefore, the cause of death was not related to the induction of mTBI. This led to a survival rate of 100% after impact which is to be expected for this height and weight (Marmarou et al., 1994). After mTBI, all rats regained consciousness within 15 min and there was no evidence of skull fractures on the CT images or at time of euthanasia (during the preparation of the histological analysis). Moreover, the anatomical T2 scans acquired after impact did not reveal any abnormalities such as enlarged ventricles, bleedings or contusions (Fig. 3). In short, we could not identify focal lesions, supporting validity for the diffuse nature of the Marmarou model.

### 3.2. In vivo longitudinal MRI changes following mTBI

Fig. 4 shows the diffusion maps of a representative mTBI rat one day after injury (FA, MD, MK, AWF, AxEAD, RadEAD and TORT). In the following paragraphs, the findings will be presented according to the diffusion model.

#### 3.2.1. Diffusion tensor imaging

As can be seen in Table 1, linear mixed model analysis revealed a significant group by time interaction effect for MD in the hippocampus and corpus callosum. Also, AD in the hippocampus and RD in the cingulum showed a significant group by time interaction effect. In the corpus callosum and hippocampus interaction effect in RD was near significant ($p = .013$ and $p = .011$, respectively). Subdividing the corpus callosum in genu, body and splenium did not reveal additional info and therefore we will discuss the corpus callosum as a total volume only and the results for genu, body and splenium can be found in

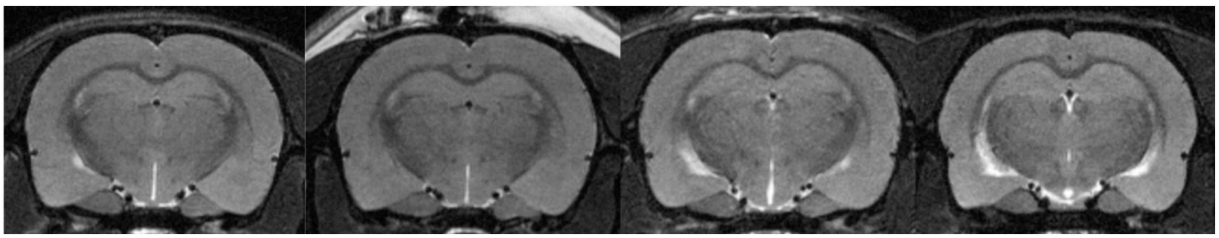

**Fig. 3.** Anatomical T2 images from left to right before (baseline), 1 day, 1 week and 3 months post injury from a representative mTBI animal.

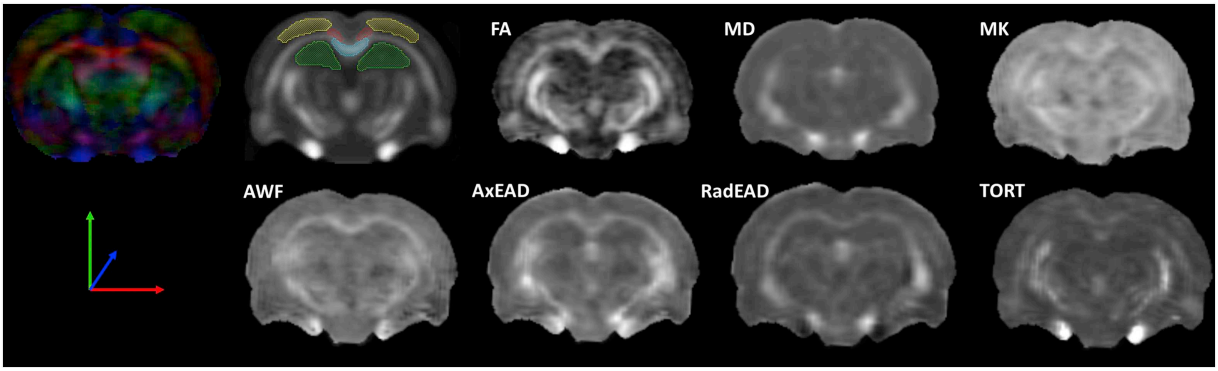


**Fig. 4.** Top row: representative coloured FA map on the left (left-right orientation: red, front-back: blue and up-down: green), the FA template with the VOIs and the FA, MD and MK map one day post impact. On the bottom row are representative images for the metrics of the white matter model. From left to right: AWF, AxEAD, RadEAD and TORT.

Table A1 of the Appendix. Post hoc tests revealed a significant decrease in MD in the hippocampus ($p$ = .008) (Fig. 5C) and in RD in the cingulum ($p$ = .010) (Fig. 6C) of the mTBI group one week post injury compared to baseline. Furthermore, RD in the cingulum stayed decreased three months post impact and was significantly lower than RD in the sham group ($p$ = .003). Also, in the corpus callosum MD was significantly lower in the mTBI group compared to sham three months post impact ($p$ = .007), in the hippocampus this was near significant ($p$ = .013). In the sham group post hoc time differences could be observed only three months post injury (Fig. 5A and C) (Table A2).

A significant main effect of time could be found for all diffusion tensor parameters across all four VOIs, with the exception of MD in the cingulum and FA in the corpus callosum, cingulum and cortex (see Table 1). This significant time effect was mostly driven by changes at the three months post injury timepoint, which represents natural developmental/aging processes and are not of particular interest in this study. Therefore, we will focus on differences at acute timepoints for the further analysis. Other significant post hoc results can be found in Table A2. In the cingulum and cortex, pairwise comparisons between baseline and one day post injury showed significant decreases in AD ($p$ = .001 and $p$ = .001, respectively) (Fig. 6B). For MD in the cortex we also obtained a decrease one day ($p$ = .001) post injury compared to

**Table 1**
*P*-values and F-values of univariate F-test for group by time interaction effect and main time effect of time in the corpus callosum, hippocampus, cingulum and cortex.

| Group by time | Corpus callosum | | Hippocampus | | Cingulum | | Cortex | |
|---|---|---|---|---|---|---|---|---|
| | F-value | *p*-value | F-value | *p*-value | F-value | *p*-value | F-value | *p*-value |
| MD | **5.961** | **0.006** | **7.185** | **0.002** | 7.485 | 0.091 | 1.024 | 0.403 |
| AD | 1.202 | 0.333 | **6.140** | **0.005** | 1.669 | 0.204 | 1.643 | 0.206 |
| RD | 5.759 | 0.013 | 4.970 | 0.011 | **7.439** | **0.010** | 1.007 | 0.041 |
| FA | 2.086 | 0.103 | 1.378 | 0.286 | 1.952 | 0.176 | 2.873 | 0.079 |
| MK | 0.327 | 0.806 | 0.658 | 0.595 | 0.459 | 0.715 | 0.603 | 0.326 |
| AK | 0.123 | 0.945 | 1.344 | 0.312 | 1.083 | 0.393 | 1.447 | 0.268 |
| RK | 0.299 | 0.926 | 0.690 | 0.573 | 0.526 | 0.671 | 0.268 | 0.848 |
| AWF | 0.203 | 0.893 | na | | 0.443 | 0.726 | na | |
| IAD | 0.353 | 0.787 | na | | 1.046 | 0.405 | na | |
| AxEAD | 0.694 | 0.569 | na | | 1.695 | 0.192 | na | |
| RadEAD | 3.622 | 0.036 | na | | **5.139** | **0.008** | na | |
| TORT | 3.539 | 0.054 | na | | 2.271 | 0.131 | na | |

| Time | Corpus callosum | | Hippocampus | | Cingulum | | Cortex | |
|---|---|---|---|---|---|---|---|---|
| | F-value | *p*-value | F-value | *p*-value | F-value | *p*-value | F-value | *p*-value |
| AD | **39.868** | **< 0.001** | **13.392** | **< 0.001** | **13.342** | **< 0.001** | **7.599** | **0.001** |
| RD | **7.105** | **0.006** | **7.711** | **0.002** | **7.724** | **0.009** | **6.512** | **0.003** |
| MD | **13.862** | **< 0.001** | **12.015** | **< 0.001** | 15.106 | 0.042 | **6.534** | **0.003** |
| FA | 3.036 | 0.045 | **17.113** | **< 0.001** | 4.063 | 0.034 | 4.342 | 0.026 |
| AK | 3.430 | 0.055 | 4.672 | 0.025 | **16.176** | **< 0.001** | **8.077** | **0.002** |
| RK | **7.906** | **0.002** | **7.116** | **0.004** | **14.750** | **< 0.001** | **5.427** | **0.010** |
| MK | **7.104** | **0.004** | **6.258** | **0.010** | **11.500** | **< 0.001** | **5.747** | **0.008** |
| AWF | **13.478** | **< 0.001** | na | | **18.533** | **< 0.001** | na | |
| IAD | 1.706 | 0.186 | na | | 3.467 | 0.048 | na | |
| AxEAD | **41.377** | **< 0.001** | na | | **20.608** | **< 0.001** | na | |
| RadEAD | **5.809** | **0.007** | na | | **10.040** | **< 0.001** | na | |
| TORT | 2.619 | 0.106 | na | | 5.667 | 0.011 | na | |

na = not applicable.
Bold indicates the p-values that are survived Bonferroni correction for multiple comparisons.

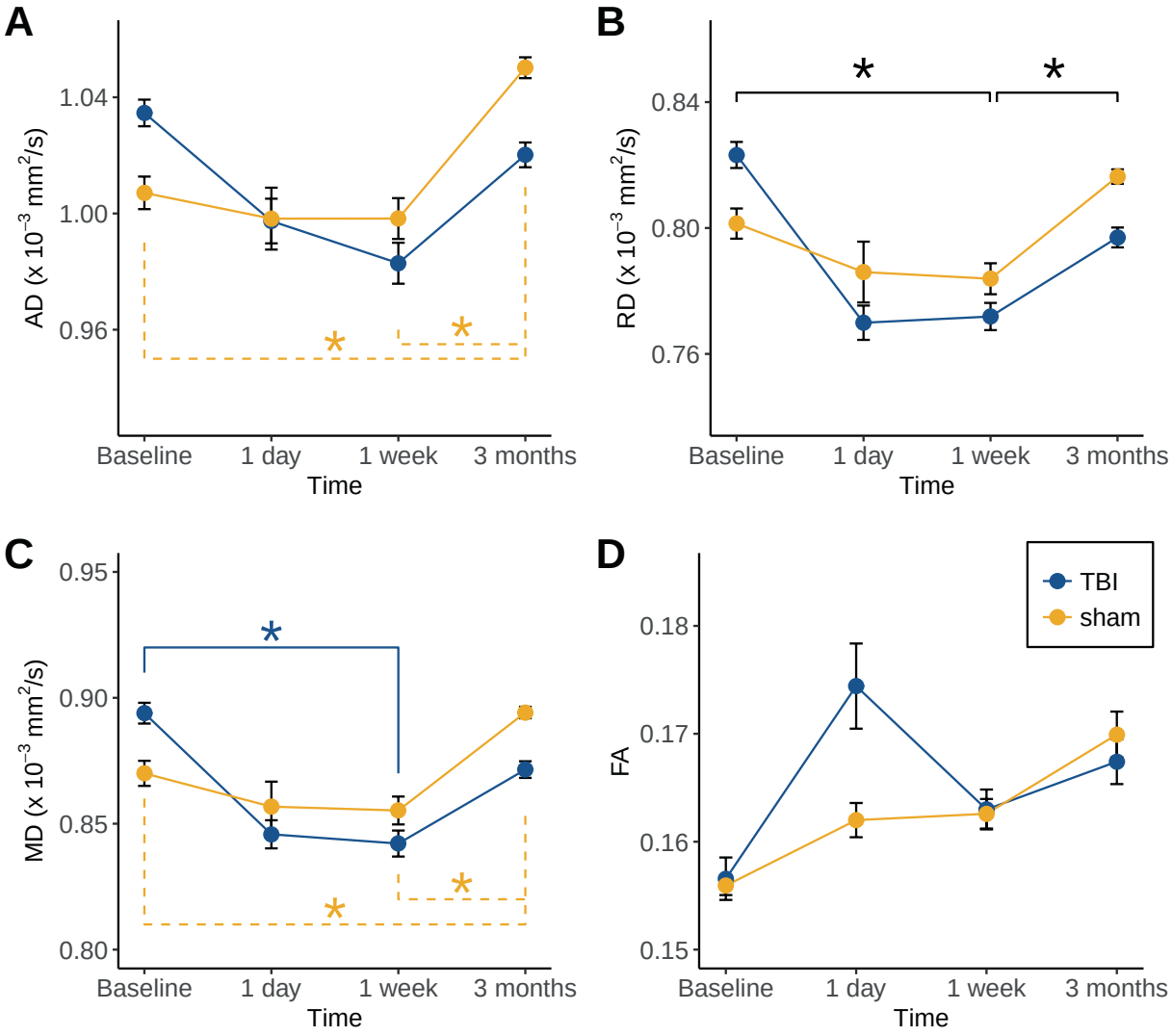


**Fig. 5.** Temporal changes in AD, RD, MD and FA in the hippocampus. *$p < .01$.

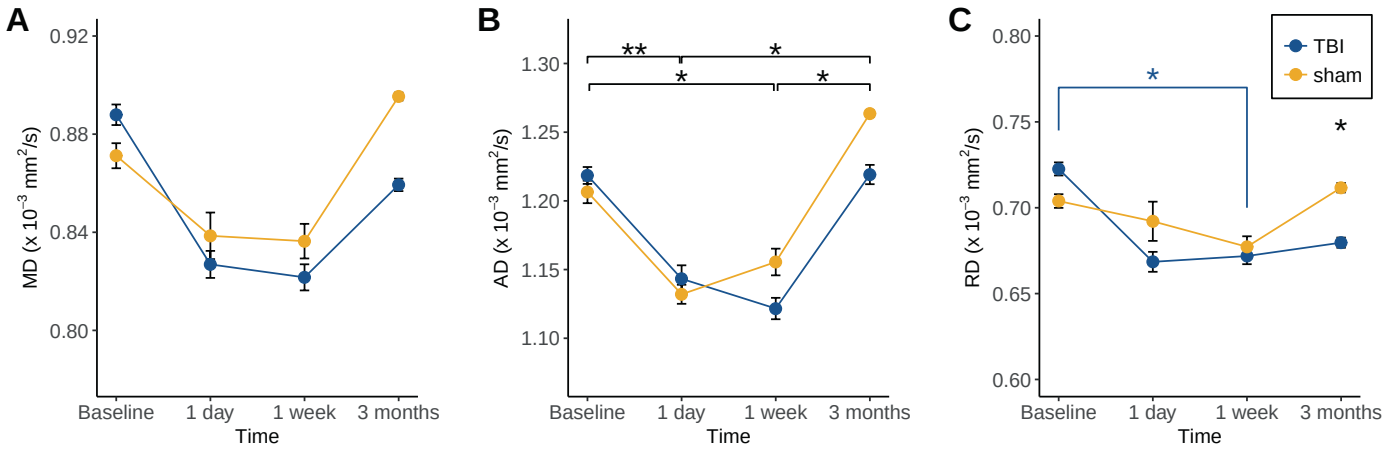


**Fig. 6.** Temporal changes in MD, AD and RD in the cingulum. *$p < .01$, **$p \leq .001$.

baseline and in the cingulum AD was decreased one week post injury compared to baseline as well ($p = .009$) (Fig. 6B). One week post injury, RD was significantly decreased in the hippocampus ($p = .008$) (Fig. 5B). All values returned towards baseline levels after three months. In the hippocampus FA showed an increase between baseline and one day post injury – especially in the mTBI group after visual inspection – and remained elevated after three months, however this effect did not survive multiple comparisons correction ($p = .023$) (Fig. 5D). In the corpus callosum we found a significant increase in AD three months post injury compared to baseline ($p < .001$). The main

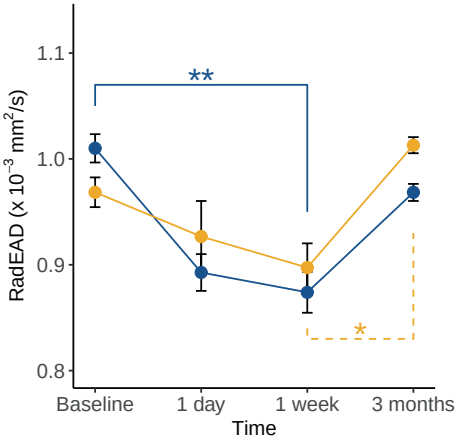


**Fig. 7.** Temporal changes RadEAD in the cingulum. *$p < .01$, **$p \leq .001$.

group effect was not significant across all DTI parameters and VOIs.

### 3.2.2. Diffusion kurtosis imaging

No significant group by time interactions effects or significant main effects of group could be demonstrated for any of the DKI parameters in any of the four VOIs. Although, AK, RK and MK values showed a significant main effect of time for the majority of the VOIs (Table 1). Post hoc tests revealed that AK of the cortex ($p = .009$) was significantly decreased after one week compared to baseline. In the hippocampus ($p = .005$) and cingulum ($p = .006$) RK was significantly decreased after one week compared to baseline which coincided with a decrease in MK in the hippocampus ($p = .007$) (Fig. A1). Similar as with the DTI parameters, the DKI parameters returned to baseline levels after three months. In the corpus callosum significant time effects were found only after three months (Table A2).

### 3.2.3. White matter model in corpus callosum and cingulum

Mixed model analysis revealed a significant interaction effect for RadEAD of the cingulum (Table 1). Post hoc tests showed that RadEAD of the cingulum was significantly decreased ($p < .001$) in the mTBI group one week post injury (Fig. 7). In the sham group this change in RadEAD could not be observed and only a significant increase between one week and three months was present ($p = .006$).

In addition, we found a significant main effect of time for AxEAD, RadEAD and AWF in the white matter bundles, IAD did not show a main effect of time except in the body of the corpus callosum ($p = .004$) (Table A1). Pairwise comparisons revealed a significant decrease in RadEAD in the corpus callosum ($p = .009$) after one week compared to baseline and these values returned to baseline levels after three months. IAD in the body of the corpus callosum did not survive multiple comparisons. Additionally, in the cingulum AxEAD was significantly decreased after one day ($p = .001$) and one week ($p = .001$) and in the corpus callosum increased ($p = .002$) after three months compared to baseline. AWF showed a significant increase in the corpus callosum ($p < .001$) and cingulum ($p = .008$) after three months compared to baseline. Main effects of group were absent.

## 3.3. Histological changes three months after injury

Fig. 8 shows sections stained with GFAP, SYN and NF of representative mTBI and sham rats. In the mTBI group, only correlation coefficients from the GFAP and NF staining in the hippocampus survived following multiple comparison correction. One day after mTBI, strong a positive correlation coefficient was observed between average pixel value of the GFAP staining and FA ($r = 0.908$–$p = .012$) in the hippocampus (Fig. 9A). This correlation indicates that high values of FA, correspond to a higher degree of glial staining. Three months post injury, we also found a positive and strong correlation between GFAP reactivity and MK values (Table 2) (Fig. 9B). Other significant correlations surviving multiple comparisons correction for GFAP can be found in Table 2. With regards to the neurofilament marker, we observed strong negative correlations between NF and AK, MD, RD and MK three months after impact (see Table 2) denoting more dephosphorylated neurofilaments at lower values of the diffusion metrics (Fig. 9C-D). In the mTBI group, no other VOIs showed significant associations surviving the multiple comparisons correction. We could only demonstrate a significant positive correlation between SYN staining and MD ($r = 0.957$–$p = .003$) in the cingulum of the sham group 3 months post impact that survived the correction for multiple comparison.

## 4. Discussion

In the present study, we demonstrated longitudinal changes in advanced diffusion MRI metrics and we revealed significant strong correlations with histopathological makers in a closed head rat model of mild TBI. We investigated structural changes after mTBI at acute time points (one day and one week post injury) and chronically (three months post injury) by linking back to pre-injury scans. Additionally, we have identified the underlying specific microstructural processes in order to establish better biomarkers for mTBI for future studies. The major findings of this study are: (1) diffusion MRI is able to follow up changes in a rat model of mTBI with no visible lesions on anatomical scans and (2) the diffusion metrics correlate with histological markers indicative of neuronal damage and glial response.

Several studies have used dMRI to follow up the complex and heterogeneous microstructural changes following mTBI, whereby DTI metrics have been used most often. In support of our findings, previous studies found decreases in diffusivity in both single and repetitive impact models throughout the brain in the first week after injury (Li et al., 2013; Qin et al., 2018; Singh et al., 2016; Sullivan et al., 2013; Yu et al., 2017; Zhuo et al., 2012). In the hippocampus and cingulum of the mTBI group, we demonstrated significant decreases in respectively MD and RD one week post injury which was already visible one day post injury (Figs. 5 and 6). Cytotoxic oedema in the acute stage can reduce the extracellular space and highly restrict water diffusion leading to decreases in diffusivity (Qin et al., 2018). Additionally, we were able to demonstrate a significant decrease in RadEAD in the cingulum one week post injury for the first time. The study by Guglielmetti et al. (2016) could also demonstrate a decrease in RadEAD along with a decrease in IAD and AxEAD in the corpus callosum following three weeks of cuprizone ingestion which induces demyelination. They hypothesised that an inflammatory response could induce infiltration of microglia and myelin debris and this way reduce the extracellular space. Inflammation could also explain the reduction in RadEAD we found in the cingulum, however we do not believe myelin debris is present in our model given the mild impact. From the present findings, it seems thus that mTBI has predominantly an influence in the cingulum and hippocampus. Furthermore, the decrease in diffusivity was mainly driven by a strong decrease in the radial components and to a lesser extent the axial components. Though, a decrease in AD has previously been described in the hippocampus, cortex, external capsule and corpus callosum 10 days post injury, the decrease in AD in the hippocampus we noticed one week post injury was not significant from baseline and we could not attribute it to the mTBI group (Table 1 and Fig. 5A) (Qin et al., 2018; Tu et al., 2016). Therefore, we suggest, as stated before, that the axonal integrity in our injury model is more or less preserved (i.e. probably there were no disrupted axons or cell debris) since diffusion along the axons changed minor. Notwithstanding, diffusion in perpendicular (radial) directions will be more restricted due to the reduced extracellular space filled with activated glial cells.

In the hippocampus we found several significant correlations between the histological markers and diffusion metrics. We observed a

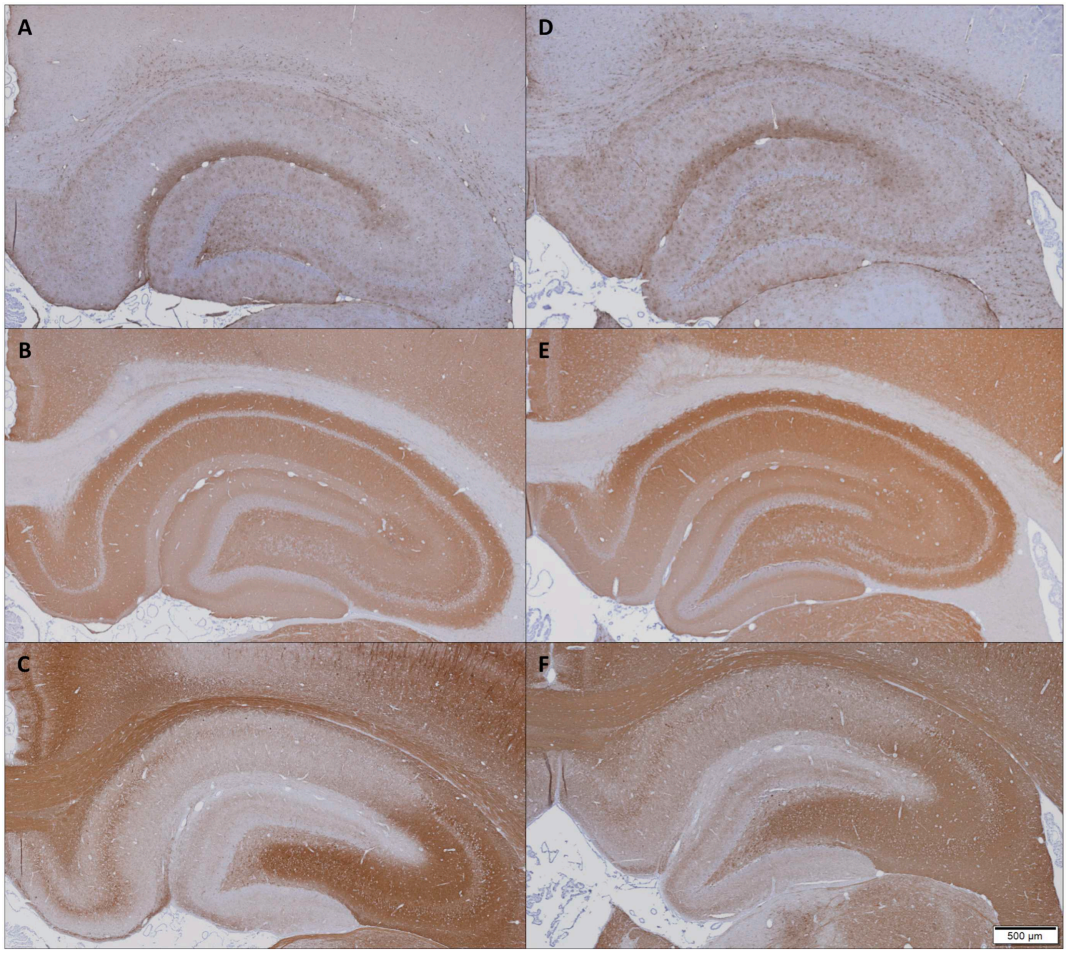


**Fig. 8.** Representative sections for Sham (left) and TBI (right) animals three months post injury. Upper row sections stained for GFAP, middle row SYN and bottom row NF.

negative correlation between NF and MD, MK and AK three months post injury, indicating a higher dephosphorylation status at lower values of diffusion or kurtosis. Neurofilaments are a major part of the neuronal cytoskeleton and provide structural support for axons to ensure optimal transport. TBI can influence the structure of the neurofilaments by altering the phosphorylation status (Siedler et al., 2014). After mTBI a secondary chemical cascade starts – even within hours of the injury – and this can activate $Ca^{2+}$ dependent proteases. These proteases can cause in their turn serious damage to the cytoskeleton and ion channels of the cells. One pathway that can mediate side chain phosphorylation of the neurofilament is led by the $Ca^{2+}$-dependent calpain and calcineurin (Johnson et al., 2013). These activated proteins can dephosphorylate the neurofilament side chains and this leads to compaction of the neurofilaments and shrinkage of the axonal space (Siedler et al., 2014). This result is in concordance with the human mTBI study by (Grossman et al., 2015), whereby reduced N-acteyl aspartate (NAA) levels coincided with decreased AWF values, which supports the hypothesis of shrinkage of the axonal space and impairments in the axonal transport. The group of Grossman et al. also revealed that NAA was negatively correlated with RadEAD and is opposite to our findings of reduced RadEAD after mTBI. We suggest that reduced radial extra-axonal diffusion could be explained by increased activity or hypertrophy of glial cells surrounding the axons. Unfortunately, correlation analysis of the cingulum did not survive multiple comparisons and we cannot confirm this hypothesis.

Apart from neurons, astrocytes also suffer from the mechanical forces that could lead to a secondary chemical cascade. Normally, astrocytes will help to maintain homeostasis but the chemical cascade can activate the astrocytes (sometimes referred to as astrogliosis) to start an inflammatory response that releases stress factors (Burda et al., 2016). One day post injury FA was (near) significantly increased in the hippocampus, and these elevated values were strongly positively correlated with GFAP – used as a marker for astrocytes – in the mTBI group. This could be explained by a higher tissue organization from astrocyte processes that form more coherent pathways. At the acute stage, (Zhuo et al., 2012) also found an increase in FA in the hippocampus, however, they did not find this increased FA to be associated with an increase in GFAP reactivity. On the contrary, they found that MK was more sensitive to changes associated with reactive gliosis. In our study, we also found that MK – and by extension also AK and RK – was highly sensitive to changes in GFAP – though at the more subacute time point (three months post injury). Thus, increased values of the kurtosis three months post injury were related to a prolonged inflammatory response and the increase in cellularity it governs. By combining increased values of FA at the acute timepoint and increased kurtosis values at later timepoints as biomarkers, we could be able to detect neuroinflammation in the hippocampus early on and monitor its progression.

It is clear from the present study that moving beyond the diffusion tensor model can bring more insights into the underlying brain changes following mTBI, i.e. the DKI metrics are more sensitive to prolonged inflammation compared to DTI metrics, and the WMTI metrics provide more specific/detailed information about the affected compartments (intra-axonal versus extra-axonal). Interestingly to note is that a couple of our findings in a mTBI rat model are not always in line with the results from human mTBI studies. As already mentioned, we observed a decrease in RadEAD that is inconsistent with the human study of

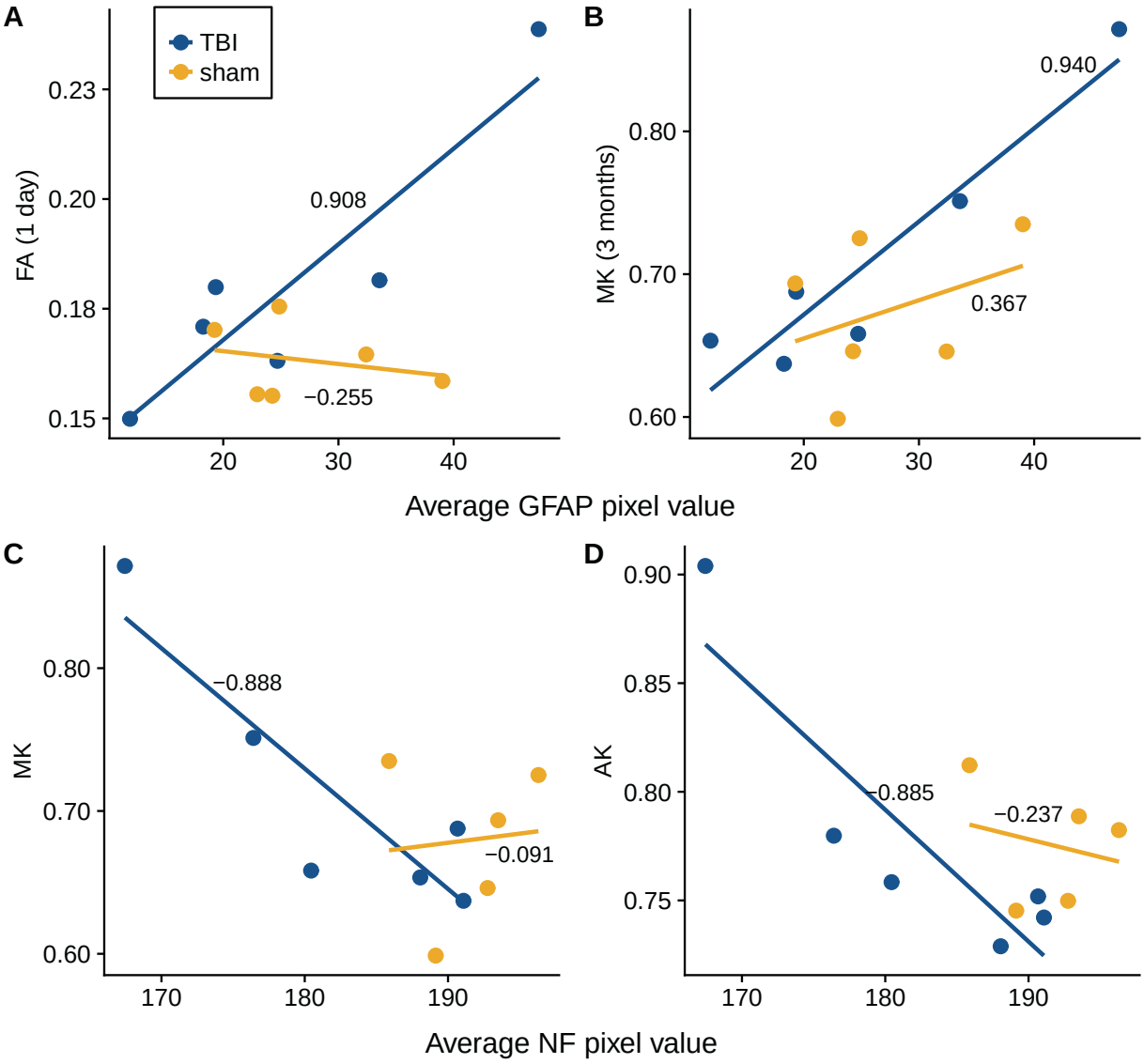


**Fig. 9.** Correlation of GFAP with FA in the hippocampus one day post impact (A) and with MK 3 months post injury (B). Correlation of NF with MK and AK in the hippocampus 3 months post injury (C-D).

**Table 2**
Significant correlations between the diffusion metrics and GFAP and NF staining in the hippocampus three months post injury.

| 3 months post injury | GFAP | | NF | |
|---|---|---|---|---|
| | r | *p*-value | r | *p*-value |
| AK | **0.943** | **0.005** | **−0.885** | **0.019** |
| RK | **0.900** | **0.014** | −0.856 | 0.030 |
| MD | 0.854 | 0.030 | **−0.902** | **0.014** |
| RD | **0.873** | **0.023** | **−0.888** | **0.018** |
| MK | **0.940** | **0.005** | **−0.888** | **0.018** |

Bold indicates the p-values that are survived Bonferroni correction for multiple comparisons.

(Grossman et al., 2015). The study by (Chung et al., 2018) demonstrated significantly lower intra-axonal diffusivity in the splenium of the corpus callosum of mTBI patients, compared with controls, but did not reveal significant changes in the radial metrics. These discrepancies in findings show that rodent models do not always translate into human studies. We suggest that future rodent models of mTBI should take into account the different mechanical forces of sustaining a TBI (coup versus rotational forces) or site of impact (frontal, temporal).

A limitation of this study is that histological sections were stained only for three markers (GFAP, NF and SYN) to investigate cellular changes. Although we demonstrated clear associations of GFAP and NF with FA and kurtosis metrics in the hippocampus, we should keep in mind that also other biophysical processes could alter the diffusion metrics after TBI. For example, demyelination could also drive the decrease in RD. However, the study by Sullivan et al. concluded that the role of demyelination after mTBI is limited and is more likely to be associated with more severe TBI (Sullivan et al., 2013). Additionally, it is becoming clearer that – apart from the way of sustaining the injury – also subtle differences in reaction of the tissue to trauma can act upon diffusion measures in complete opposite ways. For example, Lipton et al. found bidirectional changes in FA throughout the white matter of the human brain (Lipton et al., 2012). A similar pattern was identified in white and grey matter in the animal study of (Harris et al., 2016). Therefore, in future studies, the association between the cellular processes and the diffusion metrics should be explored further, in order to

fully understand the relation between them throughout the brain. This will enable us to identify a biomarker that can classify a patient with mTBI and also identify the underlying cellular damage of the affected brain regions. It should also be noted that we observed significant main effect of time in several DTI and DKI metrics. This time effect was mostly driven by changes at the three-month timepoint and could be explained by early aging processes. Specifically, we observed increased MD and increased DKI-related metrics, in both mTBI and sham groups, between the one-week and three-month time points. We interpret this alterations in MD and DKI-related metrics as early aging processes, which is consistent with previous diffusion MRI studies over the lifespan (Billiet et al., 2015; Lebel et al., 2012, 2017). Lastly, we noted a large inter subject variability, especially in the kurtosis and white matter metrics – which is common for the technique – which makes it difficult to detect group differences (De Santis et al., 2014; Szczepankiewicz et al., 2013). In our study, we found this especially challenging since the mTBI induces an effect size that cannot always overcome the inter subject variability and possible scanner fluctuations in this relatively small sample size. It is therefore possible that we missed small but relevant effects and we are now limited to finding only the large effects.

## 5. Conclusion

Despite the aforementioned limitations, we were able to demonstrate that both DTI and more advanced diffusion models are sensitive in detecting longitudinal changes after mTBI and that the diffusion metrics can be linked with cellular processes. Our results revealed significant decreases in radial metrics in the cingulum and MD in the hippocampus one week after impact only in the mTBI group, which can be connected to cellular swelling, without major changes in axial metrics, which suggests that the axon integrity is preserved. Additionally, we observed high correlations between FA from the diffusion tensor model one day post injury and an increased GFAP reactivity in the hippocampus, indicating a prolonged inflammatory response. Therefore, we think that FA and radial diffusivity might be promising predictive biomarkers, which could be sensitive to identify specific microstructural changes in the early phase after a mild impact.

## Acknowledgement

We would like to thank Jelle Veraart for the optimization of the Matlab code to estimate the DKI and WMTI parameters.

## Funding

This work was supported by the Research Foundation – Flanders (FWO) [grant number G027815N].

## Declaration of interest

None.

## Appendix A. Appendix

Table A1
F-values and *p*-values for group by time effect and time effect in the body, genu and splenium of the corpus callosum.

| Group by time | Body | | Genu | | Splenium | |
|---|---|---|---|---|---|---|
| | F-value | *p*-value | F-value | *p*-value | F-value | *p*-value |
| MD | 5.381 | 0.035 | 4.145 | 0.040 | 1.012 | 0.409 |
| AD | 1.936 | 0.169 | 0.566 | 0.648 | 0.662 | 0.585 |
| RD | 4.953 | 0.036 | 3.628 | 0.048 | 4.622 | 0.022 |
| FA | 1.957 | 0.208 | 0.911 | 0.465 | 2.528 | 0.107 |
| MK | 0.478 | 0.703 | 2.287 | 0.120 | 0.212 | 0.887 |
| AK | 0.335 | 0.801 | 0.342 | 0.795 | 1.099 | 0.388 |
| RK | 0.449 | 0.722 | 0.300 | 0.825 | 0.201 | 0.894 |
| AWF | 0.262 | 0.851 | 1.611 | 0.227 | 0.386 | 0.764 |
| IAD | 0.544 | 0.656 | 2.269 | 0.128 | 1.393 | 0.274 |
| AxEAD | 1.194 | 0.353 | 0.618 | 0.615 | 0.884 | 0.483 |
| RadEAD | 1.316 | 0.312 | 1.582 | 0.245 | 0.505 | 0.687 |
| TORT | 3.902 | 0.038 | 4.268 | 0.026 | 3.266 | 0.054 |
| **Time** | **Body** | | **Genu** | | **Splenium** | |
| | F-value | *p*-value | F-value | *p*-value | F-value | *p*-value |
| AD | **29.530** | **< 0.001** | **14.107** | **< 0.001** | 1.076 | 0.380 |
| RD | 6.504 | 0.019 | 4.659 | 0.024 | 1.867 | 0.187 |
| MD | **15.447** | **0.002** | **13.720** | **0.001** | 0.630 | 0.604 |
| FA | 3.861 | 0.063 | 0.608 | 0.623 | 1.375 | 0.298 |
| AK | 5.161 | 0.019 | 3.091 | 0.060 | 2.551 | 0.106 |
| RK | **8.601** | **0.002** | **6.084** | **0.006** | 5.200 | 0.015 |
| MK | **8.317** | **0.002** | **8.506** | **0.001** | **9.381** | **0.001** |
| AWF | **12.576** | **< 0.001** | **6.407** | **0.005** | **10.034** | **0.001** |
| IAD | **5.331** | **0.004** | 0.482 | 0.700 | 2.249 | 0.114 |
| AxEAD | **38.696** | **< 0.001** | **9.416** | **0.001** | 3.533 | 0.059 |
| RadEAD | **245.107** | **< 0.001** | **773.078** | **< 0.001** | **627.759** | **< 0.001** |
| TORT | 1.410 | 0.289 | 3.138 | 0.061 | 3.143 | 0.060 |

Bold indicates the p-values that are survived Bonferroni correction for multiple comparisons.

Table A2
P-values for the post hoc comparisons for main time effect for corpus callosum, hippocampus, cingulum, cortex and body, genu and splenium of the corpus callosum.

| Time | Post hoc test | Corpus callosum | Hippocampus | Cingulum | Cortex | Body | Genu | Splenium |
|---|---|---|---|---|---|---|---|---|
| | | *p*-value | *p*-value | *p*-value | *p*-value | *p*-value | *p*-value | *p*-value |
| AD | 1d – 3m | < 0.001 | ns | < 0.001 | ns | < 0.001 | < 0.001 | ns |
| | 1w – 3m | < 0.001 | | < 0.001 | | < 0.001 | ns | |
| MD | 1d – 3m | 0.002 | ns | ns | ns | 0.004 | ns | ns |
| | 1w – 3m | 0.002 | 0.001 | | | 0.005 | | |
| RD | 1w – 3m | ns | 0.003 | ns | ns | ns | ns | ns |
| AK | 1d – 3m | ns | ns | < 0.001 | ns | ns | ns | ns |
| | 1w – 3m | | | < 0.001 | 0.003 | | | |
| RK | 1d – 3m | ns | ns | < 0.001 | ns | ns | ns | ns |
| | 1w – 3m | 0.007 | | 0.001 | | 0.004 | 0.004 | |
| MK | 1d – 3m | ns | ns | 0.001 | ns | ns | ns | ns |
| | 1w – 3m | 0.007 | | 0.002 | | 0.003 | 0.010 | |
| AxEAD | 1d – 3m | < 0.001 | na | < 0.001 | na | < 0.001 | 0.009 | ns |
| | 1w – 3m | < 0.001 | | < 0.001 | | < 0.001 | ns | |
| RadEAD | 1w – 3m | 0.003 | | < 0.001 | | 0.006 | ns | ns |
| AWF | 1d – 3m | 0.004 | | < 0.001 | | 0.004 | ns | ns |
| | 1w – 3m | 0.002 | | 0.001 | | 0.001 | | 0.006 |

ns = not significant.
na = not applicable.
Note: FA and IAD did not show any significant post hoc results.

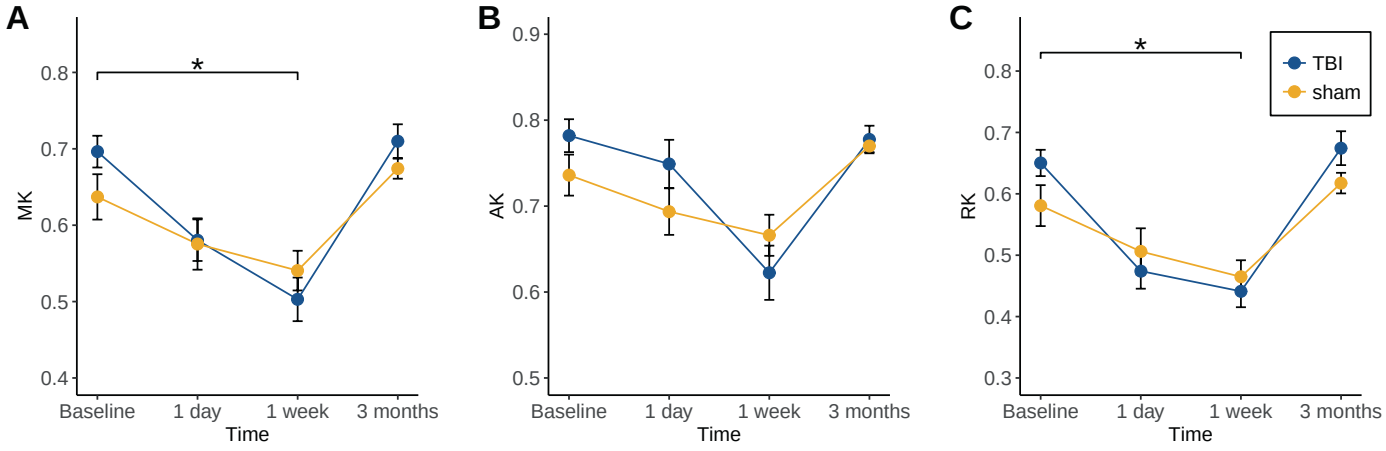


**Fig. A1.** Temporal changes in MK, AK and RK in the hippocampus. * $p < .01$.

## References


Arciniegas, D.B., Held, K., Wagner, P., 2002. Cognitive impairment following traumatic brain injury. Curr. Treat. Options Neurol. 4, 43–57. https://doi.org/10.1007/s11940-002-0004-6.

Asken, B.M., DeKosky, S.T., Clugston, J.R., Jaffee, M.S., Bauer, R.M., 2018. Diffusion tensor imaging (DTI) findings in adult civilian, military, and sport-related mild traumatic brain injury (mTBI): a systematic critical review. Brain Imaging Behav. 12, 585–612. https://doi.org/10.1007/s11682-017-9708-9.

Basser, P.J., Mattiello, J., LeBihan, D., 1994. MR diffusion tensor spectroscopy and imaging. Biophys. J. 66, 259–267. https://doi.org/10.1016/S0006-3495(94)80775-1.

Bazarian, J.J., Zhu, T., Blyth, B., Borrino, A., Zhong, J., 2012. Subject-specific changes in brain white matter on diffusion tensor imaging after sports-related concussion. Magn. Reson. Imaging 30, 171–180. https://doi.org/10.1016/j.mri.2011.10.001.

Billiet, T., Vandenbulcke, M., Mädler, B., Peeters, R., Dhollander, T., Zhang, H., Deprez, S., Van den Bergh, B.R.H., Sunaert, S., Emsell, L., 2015. Age-related microstructural differences quantified using myelin water imaging and advanced diffusion MRI. Neurobiol. Aging 36, 2107–2121. https://doi.org/10.1016/j.neurobiolaging.2015.02.029.

Bruns, J., Hauser, W.A., 2003. The epidemiology of traumatic brain injury: a review. Epilepsia 44, 2–10. https://doi.org/10.1046/j.1528-1157.44.s10.3.x.

Burda, J.E., Bernstein, A.M., Sofroniew, M.V., 2016. Astrocyte roles in traumatic brain injury. Exp. Neurol. 275, 305–315. https://doi.org/10.1016/j.expneurol.2015.03.020.

Chung, S., Fieremans, E., Wang, X., Kucukboyaci, N.E., Morton, C.J., Babb, J., Amorapanth, P., Foo, F.-Y.A., Novikov, D.S., Flanagan, S.R., Rath, J.F., Lui, Y.W., 2018. White matter tract integrity: an indicator of axonal pathology after mild traumatic brain injury. J. Neurotrauma 35, 1015–1020. https://doi.org/10.1089/neu.2017.5320.

De Santis, S., Drakesmith, M., Bells, S., Assaf, Y., Jones, D.K., 2014. Why diffusion tensor MRI does well only some of the time: variance and covariance of white matter tissue microstructure attributes in the living human brain. NeuroImage 89, 35–44. https://doi.org/10.1016/j.neuroimage.2013.12.003.

Dewan, M.C., Mummareddy, N., Wellons, J.C., Bonfield, C.M., 2016. Epidemiology of global pediatric traumatic brain injury: qualitative review. World Neurosurg 91, 497–509. e1. https://doi.org/10.1016/j.wneu.2016.03.045.

Duricki, D.A., Soleman, S., Moon, L.D.F., 2016. Analysis of longitudinal data from animals with missing values using SPSS. Nat. Protoc. 11, 1112–1129. https://doi.org/10.1038/nprot.2016.048.

Fieremans, E., Benitez, A., Jensen, J.H., Falangola, M.F., Tabesh, A., Deardorff, R.L., Spampinato, M.V.S., Babb, J.S., Novikov, D.S., Ferris, S.H., Helpern, J.A., 2013. Novel white matter tract integrity metrics sensitive to Alzheimer disease progression. Am. J. Neuroradiol. 34, 2105–2112. https://doi.org/10.3174/ajnr.A3553.

Fieremans, E., Jensen, J.H., Helpern, J.A., 2011. White matter characterization with diffusional kurtosis imaging. NeuroImage 58, 177–188. https://doi.org/10.1016/j.neuroimage.2011.06.006.

Grossman, E.J., Ge, Y., Jensen, J.H., Babb, J.S., Miles, L., Reaume, J., Silver, J.M., Grossman, R.I., Inglese, M., 2012. Thalamus and cognitive impairment in mild traumatic brain injury: a diffusional Kurtosis imaging study. J. Neurotrauma 29, 2318–2327. https://doi.org/10.1089/neu.2011.1763.

Grossman, E.J., Jensen, J.H., Babb, J.S., Chen, Q., Tabesh, A., Fieremans, E., Xia, D., Inglese, M., Grossman, R.I., 2013. Cognitive impairment in mild traumatic brain injury: a longitudinal diffusional kurtosis and perfusion imaging study. AJNR Am. J. Neuroradiol. 34, 951–957. https://doi.org/10.3174/ajnr.A3358.

Grossman, E.J., Kirov, I.I., Gonen, O., Novikov, D.S., Davitz, M.S., Lui, Y.W., Grossman, R.I., Inglese, M., Fieremans, E., 2015. N-acetyl-aspartate levels correlate with intra-axonal compartment parameters from diffusion MRI. NeuroImage 118, 334–343. https://doi.org/10.1016/j.neuroimage.2015.05.061.

Guglielmetti, C., Veraart, J., Roelant, E., Mai, Z., Daans, J., Van Audekerke, J., Naeyaert, M., Vanhoutte, G., Delgado y Palacios, R., Praet, J., Fieremans, E., Ponsaerts, P., Sijbers, J., Van der Linden, A., Verhoye, M., 2016. Diffusion kurtosis imaging probes cortical alterations and white matter pathology following cuprizone induced demyelination and spontaneous remyelination. NeuroImage 125, 363–377. https://doi.org/10.1016/j.neuroimage.2015.10.052.

Harris, N.G., Verley, D.R., Gutman, B.A., Sutton, R.L., 2016. Bi-directional changes in fractional anisotropy after experiment TBI: disorganization and reorganization? NeuroImage 133, 129–143. https://doi.org/10.1016/j.neuroimage.2016.03.012.

Hulkower, M.B., Poliak, D.B., Rosenbaum, S.B., Zimmerman, M.E., Lipton, M.L., 2013. A decade of DTI in traumatic brain injury: 10 years and 100 articles later. Am. J. Neuroradiol. 34, 2064–2074. https://doi.org/10.3174/ajnr.A3395.

Hutchinson, E.B., Schwerin, S.C., Avram, A.V., Juliano, S.L., Pierpaoli, C., 2018. Diffusion MRI and the detection of alterations following traumatic brain injury. J. Neurosci. Res. 96, 612–625. https://doi.org/10.1002/jnr.24065.

Jelescu, I.O., Zurek, M., Winters, K.V., Veraart, J., Rajaratnam, A., Kim, N.S., Babb, J.S., Shepherd, T.M., Novikov, D.S., Kim, S.G., Fieremans, E., 2016. In vivo quantification of demyelination and recovery using compartment-specific diffusion MRI metrics validated by electron microscopy. NeuroImage 132, 104–114. https://doi.org/10.1016/j.neuroimage.2016.02.004.

Jensen, J.H., Helpern, J.A., 2010. MRI quantification of non-Gaussian water diffusion by kurtosis analysis. NMR Biomed. 23, 698–710. https://doi.org/10.1002/nbm.1518.

Johnson, V.E., Stewart, W., Smith, D.H., 2013. Axonal pathology in traumatic brain injury. Exp. Neurol. 246, 35–43. https://doi.org/10.1016/j.expneurol.2012.01.013.

Jones, D.K., Knösche, T.R., Turner, R., 2013. White matter integrity, fiber count, and other fallacies: the do's and don'ts of diffusion MRI. NeuroImage 73, 239–254. https://doi.org/10.1016/j.neuroimage.2012.06.081.

Kelm, N.D., West, K.L., Carson, R.P., Gochberg, D.F., Ess, K.C., Does, M.D., 2016. Evaluation of diffusion kurtosis imaging in ex vivo hypomyelinated mouse brains. NeuroImage 124, 612–626. https://doi.org/10.1016/j.neuroimage.2015.09.028.

de Kouchkovsky, I., Fieremans, E., Fleysher, L., Herbert, J., Grossman, R.I., Inglese, M., 2016. Quantification of normal-appearing white matter tract integrity in multiple sclerosis: a diffusion kurtosis imaging study. J. Neurol. 263, 1146–1155. https://doi.org/10.1007/s00415-016-8118-z.

Lazar, M., Miles, L.M., Babb, J.S., Donaldson, J.B., 2014. Axonal deficits in young adults with high functioning autism and their impact on processing speed. NeuroImage Clin. 4, 417–425. https://doi.org/10.1016/j.nicl.2014.01.014.

Lebel, C., Gee, M., Camicioli, R., Wieler, M., Martin, W., Beaulieu, C., 2012. Diffusion tensor imaging of white matter tract evolution over the lifespan. NeuroImage 60, 340–352. https://doi.org/10.1016/j.neuroimage.2011.11.094.

Lebel, C., Treit, S., Beaulieu, C., 2017. A review of diffusion MRI of typical white matter development from early childhood to young adulthood. NMR Biomed, e3778. https://doi.org/10.1002/nbm.3778.

Leemans, A., Jeurissen, B., Sijbers, J., Jones, D., 2009. ExploreDTI: a graphical toolbox for processing, analyzing, and visualizing diffusion MR data. Proc Intl Soc Mag Reson Med 17, 3537.

Li, X.-Y., Feng, D.-F., 2009. Diffuse axonal injury: novel insights into detection and treatment. J. Clin. Neurosci. 16, 614–619. https://doi.org/10.1016/j.jocn.2008.08.005.

Li, S., Sun, Y., Shan, D., Feng, B., Xing, J., Duan, Y., Dai, J., Lei, H., Zhou, Y., 2013. Temporal profiles of axonal injury following impact acceleration traumatic brain injury in rats—A comparative study with diffusion tensor imaging and morphological analysis. Int. J. Legal Med. 127, 159–167. https://doi.org/10.1007/s00414-012-0712-8.

Lipton, M.L., Kim, N., Park, Y.K., Hulkower, M.B., Gardin, T.M., Shifteh, K., Kim, M., Zimmerman, M.E., Lipton, R.B., Branch, C.A., 2012. Robust detection of traumatic axonal injury in individual mild traumatic brain injury patients: intersubject variation, change over time and bidirectional changes in anisotropy. Brain Imaging Behav. 6, 329–342. https://doi.org/10.1007/s11682-012-9175-2.

Loening, A.M., Gambhir, S.S., 2003. AMIDE: a free software tool for multimodality medical image analysis. Mol. Imaging 2, 131–137. https://doi.org/10.1162/153535003322556877.

Marmarou, A., Foda, M.A.A.-E., van den Brink, W., Campbell, J., Kita, H., Demetriadou, K., 1994. A new model of diffuse brain injury in rats. J. Neurosurg. 80, 291–300. https://doi.org/10.3171/jns.1994.80.2.0291.

Mayer, A.R., Ling, J., Mannell, M.V., Gasparovic, C., Phillips, J.P., Doezema, D., Reichard, R., Yeo, R.A., 2010. A prospective diffusion tensor imaging study in mild traumatic brain injury. Neurology 74, 643–650. https://doi.org/10.1212/WNL.0b013e3181d0ccdd.

McDonald, J.H., 2014. Multiple comparisons. In: Handbook of Biological Statistics. Sparky House Publishing, Baltimore, Maryland, pp. 254–263.

Niogi, S.N., Mukherjee, P., Ghajar, J., Johnson, C., Kolster, R.A., Sarkar, R., Lee, H., Meeker, M., Zimmerman, R.D., Manley, G.T., McCandliss, B.D., 2008. Extent of microstructural white matter injury in postconcussive syndrome correlates with impaired cognitive reaction time: a 3T diffusion tensor imaging study of mild traumatic brain injury. Am. J. Neuroradiol. 29, 967–973. https://doi.org/10.3174/ajnr.A0970.

Novikov, D.S., Kiselev, V.G., Jespersen, S.N., 2018. On modeling. Magn. Reson. Med. 79, 3172–3193. https://doi.org/10.1002/mrm.27101.

Pierpaoli, C., Basser, P.J., 1996. Toward a quantitative assessment of diffusion anisotropy. Magn. Reson. Med. 36, 893–906. https://doi.org/10.1002/mrm.1910360612.

Qin, Y., Li, G.-L., Xu, X.-H., Sun, Z.-Y., Gu, J.-W., Gao, F.-B., 2018. Brain structure alterations and cognitive impairment following repetitive mild head impact: an in vivo MRI and behavioral study in rat. Behav. Brain Res. 340, 41–48. https://doi.org/10.1016/j.bbr.2016.08.008.

Rutgers, D.R., Toulgoat, F., Cazejust, J., Fillard, P., Lasjaunias, P., Ducreux, D., 2008. White matter abnormalities in mild traumatic brain injury: a diffusion tensor imaging study. Am. J. Neuroradiol. 29, 514–519. https://doi.org/10.3174/ajnr.A0856.

Siedler, D.G., Chuah, M.I., Kirkcaldie, M.T.K., Vickers, J.C., King, A.E., 2014. Diffuse axonal injury in brain trauma: insights from alterations in neurofilaments. Front. Cell. Neurosci. 8, 429. https://doi.org/10.3389/fncel.2014.00429.

Singh, K., Trivedi, R., Devi, M.M., Tripathi, R.P., Khushu, S., 2016. Longitudinal changes in the DTI measures, anti-GFAP expression and levels of serum inflammatory cytokines following mild traumatic brain injury. Exp. Neurol. 275, 427–435. https://doi.org/10.1016/j.expneurol.2015.07.016.

Sullivan, G.M., Mierzwa, A.J., Kijpaisalratana, N., Tang, H., Wang, Y., Song, S.-K., Selwyn, R., Armstrong, R.C., 2013. Oligodendrocyte lineage and subventricular zone response to traumatic axonal injury in the corpus callosum. J. Neuropathol. Exp. Neurol. 72, 1106–1125. https://doi.org/10.1097/NEN.0000000000000009.

Szczepankiewicz, F., Lätt, J., Wirestam, R., Leemans, A., Sundgren, P., van Westen, D., Ståhlberg, F., Nilsson, M., 2013. Variability in diffusion kurtosis imaging: impact on study design, statistical power and interpretation. NeuroImage 76, 145–154. https://doi.org/10.1016/j.neuroimage.2013.02.078.

Thurman, D.J., 2016. The epidemiology of traumatic brain injury in children and youths. J. Child Neurol. 31, 20–27. https://doi.org/10.1177/0883073814544363.

Tu, T.-W., Williams, R.A., Lescher, J.D., Jikaria, N., Turtzo, L.C., Frank, J.A., 2016. Radiological-pathological correlation of diffusion tensor and magnetization transfer imaging in a closed head traumatic brain injury model. Ann. Neurol. 79, 907–920. https://doi.org/10.1002/ana.24641.

Veraart, J., Fieremans, E., Novikov, D.S., 2016. Diffusion MRI noise mapping using random matrix theory. Magn. Reson. Med. 76, 1582–1593. https://doi.org/10.1002/mrm.26059.

Veraart, J., Novikov, D.S., Christiaens, D., Ades-aron, B., Sijbers, J., Fieremans, E., 2016. Denoising of diffusion MRI using random matrix theory. NeuroImage 142, 394–406. https://doi.org/10.1016/j.neuroimage.2016.08.016.

Veraart, J., Poot, D.H.J., Van Hecke, W., Blockx, I., Van der Linden, A., Verhoye, M., Sijbers, J., 2011. More accurate estimation of diffusion tensor parameters using diffusion kurtosis imaging. Magn. Reson. Med. 65, 138–145. https://doi.org/10.1002/mrm.22603.

Veraart, J., Sijbers, J., Sunaert, S., Leemans, A., Jeurissen, B., 2013. Weighted linear least squares estimation of diffusion MRI parameters: strengths, limitations, and pitfalls. NeuroImage 81, 335–346. https://doi.org/10.1016/j.neuroimage.2013.05.028.

Wallace, E.J., Mathias, J.L., Ward, L., 2018. Diffusion tensor imaging changes following mild, moderate and severe adult traumatic brain injury: a meta-analysis. Brain Imaging Behav 1–15. https://doi.org/10.1007/s11682-018-9823-2.

Yu, F., Shukla, D.K., Armstrong, R.C., Marion, C.M., Radomski, K.L., Selwyn, R.G., Dardzinski, B.J., 2017. Repetitive model of mild traumatic brain injury produces cortical abnormalities detectable by magnetic resonance diffusion imaging, histopathology, and behavior. J. Neurotrauma 34, 1364–1381. https://doi.org/10.1089/neu.2016.4569.

Zhang, S., Zhang, J., Fang, J., Liang, M., Li, J., Wang, X., Zhou, Q., 2018. Preliminary study of diffusion kurtosis imaging in mild traumatic brain injury. Iran. J. Radiol. 15, 1–10. https://doi.org/10.5812/iranjradiol.56115.Research.

Zhuo, J., Xu, S., Proctor, J.L., Mullins, R.J., Simon, J.Z., Fiskum, G., Gullapalli, R.P., 2012. Diffusion kurtosis as an in vivo imaging marker for reactive astrogliosis in traumatic brain injury. NeuroImage 59, 467–477. https://doi.org/10.1016/j.neuroimage.2011.07.050.